This is an open access article published under an ACS AuthorChoice License, which permits copying and redistribution of the article or any adaptations for non-commercial purposes.

ACS AuthorChoice

Langmuir

Letter

pubs.acs.org/Langmuir

Controlled Self-Assembly of Hexagonal Nanoparticle Patterns on Nanotopographies

Laith F. Kadem, Constanze Lamprecht, Julia Purtov, and Christine Selhuber-Unkel*

Institute for Materials Science, Biocompatible Nanomaterials, University of Kiel, Kaiserstr. 2, Kiel 24143, Germany

S *Supporting Information*

ABSTRACT: Diblock copolymer micelle nanolithography (BCML) is a versatile and efficient method to cover large surface areas with hexagonally ordered arrays of metal nanoparticles, in which the nanoparticles are equally spaced. However, this method falls short of providing a controlled allocation of such regular nanoparticle arrays with specific spacing into micropatterns. We present here a quick and high-throughput method to generate quasi-hexagonal nanoparticle structures with well-defined interparticle spacing on segments of nanotopographic Si substrates. The topographic height of these segments plays a dominant role in dictating the spacing between the gold nanoparticles, as the nanoparticle arrangement is controlled by immersion forces and by their self-assembly within the segments. Our novel strategy of employing a single-step BCML routine is a highly promising method for the fabrication of regular gold nanopatterns in micropatterns for a wide range of applications.

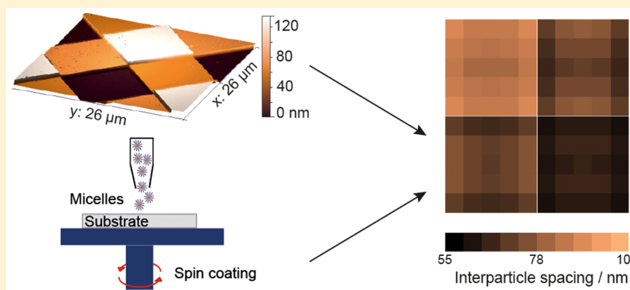

1. INTRODUCTION

Block copolymer micelle nanolithography (BCML) has proven versatile in generating quasi-hexagonally arranged patterns of metal nanoparticles on a variety of surfaces, including silicon and glass,[1] Teflon,[2] and even hydrogels.[3] Such substrates are employed in a large number of applications such as biomimetic optics,[4] protein binding,[5] and controlled cell adhesion[6−8] to name a few. In BCML, block copolymers that consist of two blocks of polymers with different polarities, most commonly polystyrene (PS) and poly-2-vinylpyridine (P2VP), are dissolved in a solvent. Above the critical micellar concentration, these block copolymers arrange into spherical micelles that can be loaded with a metallic precursor.[9] By dip or spin coating the micelle solution onto flat substrates, the loaded micelles self-assemble into quasi-hexagonal patterns, and after removal of the micellar polymer shell by plasma treatment, quasi-hexagonally ordered arrays of metal nanoparticles remain on the surface.[10] The lateral spacing between the nanoparticles can be varied by controlling the molecular weight of the diblock copolymers, the polymer concentration, and the coating speed during deposition of the micelle solution.[11] For example, increasing the rotational speed during spin coating reduces the thickness of the micelle-containing liquid film on the surface and results in a lower density of packed micelles, which leads to larger interparticle spacing. The nanoparticle size itself is controlled by the amount of metallic precursor and can additionally be increased by electroless deposition.[12]

Superposition of the quasi-hexagonal nanopattern generated with BCML with an additional microstructure to form so-called micronanostructures would be advantageous in many applications. Living cells, for example, have the remarkable ability to react on both biofunctionalized nanopatterns[6] and microstructures.[13] Furthermore, other applications such as DNA chips,[14] nanowire fabrication,[15] and optically active nanocoatings[4] would benefit from a controlled spacing of gold nanoparticles on the microscale. So far, the combination of BCML-fabricated nanopatterns and microstructures to form micronanostructures includes conventional electron beam lithography[16] and photolithography[17] top-down procedures. The BCML-based micronanostructures created with these techniques are typically restricted to microscale areas that contain a specific spacing of gold nanoparticles separated by uncoated areas.[18] The fabrication of micronanostructures with neighboring areas of different gold nanoparticle spacings would be extremely time-consuming with this approach, as it requires several coating and lithography steps.[19] In addition, precise alignment between the different lithography and BCML steps would be a major hurdle. Altogether, the fabrication of micronanostructures in a simple and high-throughput process that generates neighboring arrays with different specific interparticle spacings remains a significant challenge.

As BCML relies on the undisturbed self-assembly of micelles on a smooth surface, it is well known that surface roughness impairs the regular hexagonal structure of nanoparticle arrays typically generated by BCML.[20] Here we propose an easy and straightforward method that explicitly makes use of this effect by introducing sharp edges onto a Si surface in order to guide the micelles into a certain microstructure. Most importantly, we

Received: June 15, 2015
Revised: August 9, 2015
Published: August 12, 2015

ACS Publications © 2015 American Chemical Society

DOI: 10.1021/acs.langmuir.5b02168
Langmuir 2015, 31, 9261−9265

use only a single BCML step to deposit gold nanoparticles on substrates and yield neighboring microarrays of quasi-hexagonal nanoparticle distributions that are significantly different in their interparticle spacing.

2. MATERIALS AND METHODS

2.1. Nanotopographies. Microstructures were generated on single-side-polished, p-doped, 4 in. Si wafers (resistivity 1−30 Ω cm) with a nominal thickness of 525 ± 25 μm (Siegert Wafer, Germany) using photolithography followed by wet etching.[21] The wafers were coated with a 1500 nm ± 5% thermally grown oxide layer. First, the Si wafers were ultrasonically cleaned for 5 min in acetone (≥99.7%, Ph.Eur., extra pure, Carl Roth, Germany) and then sonicated again in isopropanol (Rotipuran ≥99.8%, p.a., ACS, ISO, Carl Roth, Germany) for another 5 min to remove the acetone before they were blown dry with N_2. Prior to applying the photoresist, wafers were treated with HMDS (hexamethyldisilazane), which helps to promote the adhesion of the resist. Afterward, a positive photoresist (AZ1518, Microchemicals, Germany) was spin coated (OPTI spin ST22P, Solar-Semi, Germany) onto the wafers at 4000 rpm, resulting in a resist layer thickness of 1.8 μm. The wafers were then taken to the mask aligner (MicroTec MA 6/BA 6, Süss, Germany) and illuminated with UV light through a chromium photomask (Compugraphics Jena, Germany) consisting of 5-μm-wide stripes with a 5 μm gap between adjacent stripes. After developing with AZ 726 MIF (Microchemicals, Germany), wafers were etched for 40 s with ammonium fluoride (ammonium fluoride etching mixture, semiconductor grade Puranal, Sigma-Aldrich, Germany) to create 5-μm-wide, 60-nm-deep stripelike grooves in the silicon dioxide layer. Eventually, the rest of the photoresist on the wafers was stripped off through ultrasonic cleaning for 5 min in acetone and then another 5 min in isopropanol, and ultimately the wafers were blown dry with N_2 (Figure 1A).

To generate the quadruple pattern, a second set of stripes was etched into the wafers by repeating the photolithography and etching steps with the photomask rotated by 90°. This procedure results in a checkerboard structure with segments of different heights (Figure 1B).

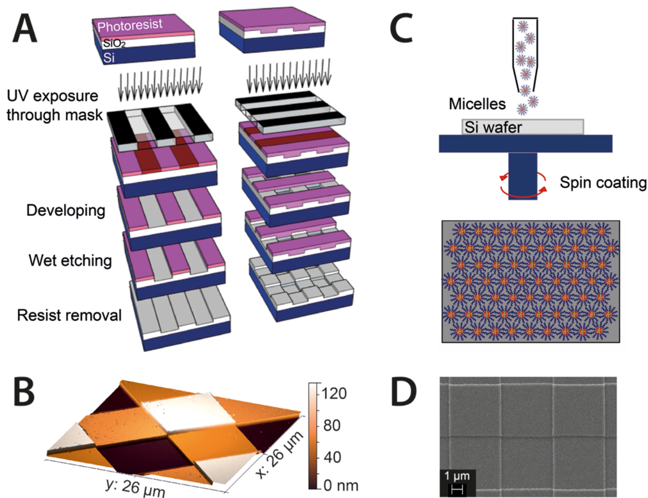

Figure 1. (A) Generation of nanotopographic Si substrates with a quadruple structure by photolithography and wet etching. (B) AFM surface scan of the patterned substrate showing 5 μm × 5 μm segments with height differences of 60 nm between adjacent segments. (C) Schematic illustration of the BCML procedure. A micelle solution is transferred onto the Si wafer in a spin coater, and micelles self-assemble on a planar substrate into a quasi-hexagonal structure. Plasma treatment removes the polymer micelles, leaving only metallic gold nanoparticles on the substrate. (D) SEM image of the nanostructured nanotopography.

2.2. Block Copolymer Micelle Nanolithography (BCML). The microstructured samples were patterned with gold particles using block copolymer micelle nanolithography. Poly(styrene-*b*-2-vinyl-pyridine) (PS(110000)-*block*-P2VP(52000), 4 mg/mL, Polymer Source, Canada) was dissolved in toluene (p.A., Merck, Germany) and loaded with tetrachlorogold(III) acid trihydrate (Aldrich, Germany) in a molecular ratio of 0.4. The Si microstructures were cleaned in an acetone ultrasonic bath for 5 min followed by a 5 min ultrasonication in isopropanol. A droplet of 20 μL of the gold-loaded polymer solution was spin coated onto the microstructured Si substrate at 1000, 5000, and 7000 rpm (WS-650Mz-23NPP, Laurell, USA). To remove the micellar polymer, the spin-coated, dry substrates were exposed to plasma using a mixture of hydrogen and argon gas (10% hydrogen, 90% argon) in a plasma etcher (TePla 100 plasma system, PVA, Germany) at 0.4 mbar and 300 W for 1 h. In order to further homogenize the micelle distribution, on specific samples ultrasound annealing was carried out for 30 s as described by Williges et al.[22]

2.3. Scanning Electron Microscopy (SEM) and Image Analysis. Prior to SEM imaging, the samples were coated with a thin layer of graphite using a sputter coater (BAL-TEC SCD 050, Capovani Brothers Inc., USA). SEM (Supra 55VP, Zeiss, Germany) imaging was carried out at 5 kV using both in-lens and secondary electron detectors at a working distance of 3 mm. The interparticle spacing was on the one hand calculated using a custom-written Matlab routine (Matlab, Mathworks, USA), which first determined the particle density and then, assuming a perfect hexagonal particle distribution, calculated the corresponding nanoparticle spacing. On the other hand, for a more accurate measurement of interparticle spacing variations as well as for calculating the 6-fold bond orientational order parameter of the nanopattern, a nearest-neighbor detection algorithm was employed in ImageJ.[22,23] Both analysis methods were performed on multiple individual areas (1 μm × 1 μm) of the same segment. Heatmaps were generated using the pcolormat function in Matlab.[24]

2.4. Atomic Force Microscopy (AFM) Imaging and Image Processing. Atomic force microscopy (AFM) topographic imaging was employed to measure the step height of Si microstructures and to determine the topography after spin coating with micelle solution. Imaging was performed on a JPK NanoWizard 3 (JPK Instruments AG) operated in ac mode using ACTA cantilevers (spring constant ∼40 N/m, resonance frequency ∼300 kHz; Applied NanoStructures Inc.) for uncoated Si microstructures and MSNL-F (spring constant ∼0.6 N/m, resonance frequency ∼100 kHz, Bruker AFM Probes) for micelle-coated samples at scan rates of 1−2.5 Hz. Image processing and cross-sectional analysis were done in Gwyddion 2.37 (Gwyddion − free SPM, sourceforge.net).

3. RESULTS AND DISCUSSION

The experimental heart of our method is a Si substrate with a microscopic quadruple surface pattern of 5 μm × 5 μm square segments. The surface was patterned using photolithography and wet etching (Figure 1A). Specifically, a 4 in. Si wafer was coated with a photoresist and irradiated with UV light through a mask consisting of stripes of 5 μm width at intervals of 5 μm. Wet etching yielded a surface topography exhibiting stripes 5 μm wide and 60 nm deep. After stripping off the resist, the wafer was again coated with a photoresist and irradiated for a second time through the mask, which had been rotated 90°. The final etching procedure resulted in a multileveled checkerboard topography of 5 μm × 5 μm segments in a quadruple pattern with a height difference of 60 nm between adjacent segments (Figure 1B). To introduce nanostructuring onto the micropatterned substrates, block copolymer micelle nanolithography was employed using a gold-carrying micelle solution that was deposited by spin coating (Figure 1C). During plasma treatment with a mixture of hydrogen and argon gases, the polymer matrix of the micelle shell was removed,

DOI: 10.1021/acs.langmuir.5b02168
Langmuir 2015, 31, 9261−9265

leaving elementary gold nanoparticles on the surface of the Si substrate. Figure 1D shows a scanning electron microscopy (SEM) image of a plasma-etched substrate that has a gold nanopattern on the nanotopographic Si substrate.

Figure 2A presents a representative magnified SEM image of the center of a quadruple segment pattern with a nanoparticle coating. The four areas of the quadruple are referred to as a, b1, b2, and c depending on the thickness of their silicon dioxide layer, with segment a being the highest, segment c being the lowest, and segments b1 and b2 being identical at an intermediate value. The image reveals visible differences in the interparticle spacing from one segment to the next. For detailed analysis, 1 μm × 1 μm spots on segments of different topographical height were examined, and the average interparticle spacing was calculated. Figure 2B shows the averaged interparticle spacings for a nanotopographic substrate spin coated at 1000 rpm, as determined with our particle-density-based algorithm. The topographically highest segment a exhibits a significantly larger average interparticle spacing than the lowest segment c, with a difference in interparticle spacing of more than 20 nm. On the other hand, segments b1 and b2 have a similar intermediate interparticle spacing. The nearest-neighbor analysis of interparticle spacing yielded comparable results [(a) 84.1 ± 9.9 nm, (b1) 71.8 ± 9.5 nm, (b2) 71.4 ± 9.5 nm, (c) 63.0 ± 10.0 nm)], where the standard deviation is a measure of the variation in spacing of individual nanoparticles.

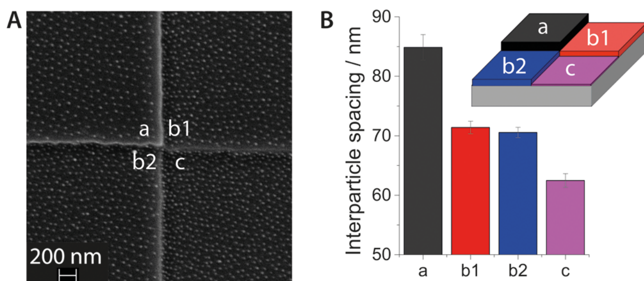

Figure 2. (A) SEM image of a gold-nanoparticle-decorated quadruple structure revealing variations in interparticle spacing between the different segments of the quadruple. (B) Interparticle spacing of nanoparticles on segments of different height, averaged from four quadruple structures. Clearly, the interparticle spacing is controlled by the segment height. The interparticle spacing was calculated from particle densities, assuming a hexagonal particle arrangement. Error bars denote the standard deviation. Inset: Color code of segments within a quadruple structure.

To explain the observed dependence of interparticle spacing on the topographical height of a segment, we also investigated the distribution of micelles on the substrate before plasma etching. At the end of the spin coating process, a monolayer of micelle solution uniformly covers the substrate and a significant difference in micelle coating density is present among the four segments (Figure 3A). Segment a is depleted in micelles at the edges bordering lower segments b1 and b2, which have the same topographical height; segments b1 and b2 are in turn depleted in micelles toward segment c, which is the lowest segment. We further analyzed height profiles of these AFM images (Figure 3B), shown as arrows in Figure 3A. These profiles prove that there is a monolayer of micelles in the center of each segment, as the height difference between the lowest and the highest segment is identical to the height difference of segments in the underlying Si microstructure. Furthermore, it shows that micelles are loosely packed on segment a, whereas micelles are densely packed on segment c. The observations are consistent with our interparticle spacing analysis of plasma-etched substrates in Figure 2. We also observe the stacking of micelles at the upward edges of the nanotopography. We suggest the arrangement of micelles to be the result of two types of forces that take effect as the solution starts to evaporate: steric interactions and immersion forces, which include drag forces due to the receding liquid surface, friction, convection, interparticle interaction, and capillary forces.[25,26] During evaporation, micelles near the edge of neighboring segments experience these immersion forces (mainly capillary and drag forces) that sweep them downward to a lower segment (Figure 3D). This results in an accumulation of larger numbers of micelles in lower segments, effectively causing higher particle densities and hence smaller interparticle spacing. It also leads to less ordered structures at the edges. As the solvent continues to evaporate, the edges of the nanotopographies act as pinpoints for menisci and capillary effects create a flux of micelle solution toward the walls. This leads to the piling up of micelles at the boundaries of lower segments compared to higher neighboring squares (Figure 3D). The graph in Figure 3C shows results from a detailed analysis of this edge effect. Our data clearly show that a depletion of nanoparticles on a topographically higher segment leads to an enrichment of nanoparticles on the adjacent lower segment.

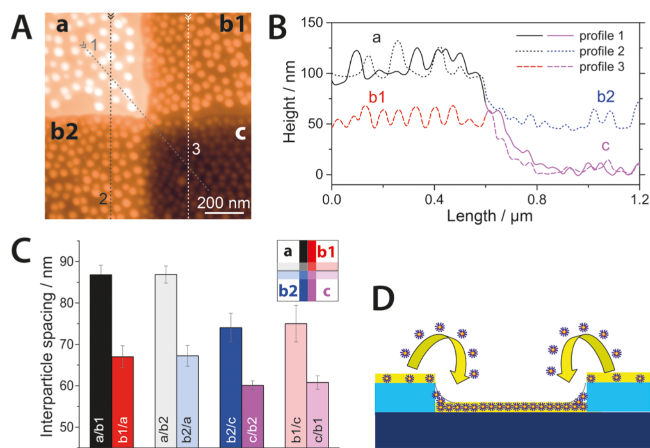

Figure 3. (A) AFM image showing the distribution of micelles after the spin coating procedure. Depletion in nanoparticles at the edge of the highest square and the enrichment of nanoparticles at the edges of lower squares are clearly visible. (B) Height profiles for lines 1, 2, and 3 shown in A revealing the stacking of micelles at the edges of lower segments. These data also prove that indeed monolayers of micelles are adsorbed on all four segments. (C) Average of interparticle spacing along a 1 μm broad stripe at the edge of different segments (x/y refers to the 1 μm broad stripe on segment x that is adjacent to segment y). The data quantify the enrichment and depletion of nanoparticles on the lower and higher segments, respectively. Furthermore, the data are consistent, as segments b1 and b2 have identical heights and lead to identical interparticle spacings. (D) Sketch of the proposed mechanism for micelle enrichment in the lower segments, caused by a flow of micelles toward the lower segments of the quadruple structure during solvent drying.

Moreover, our study demonstrates a clear correlation between the organization and spacing of nanoparticles on the one hand and the spin coating speed used during preparation on the other hand. Figure 4 shows that an increase in spin coating speed induces an increase in interparticle spacing, in

DOI: 10.1021/acs.langmuir.5b02168
Langmuir 2015, 31, 9261−9265

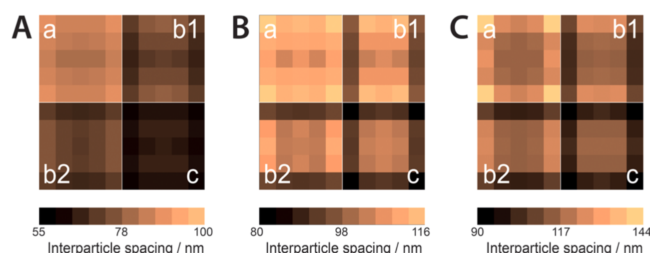

Figure 4. Heat maps showing how nanoparticle spacing is controlled by the nanotopography and by the spin coating speed. Increasing the spin coating speed causes an overall increase in interparticle spacing. A spin coating speed of 1000 rpm leads to an almost homogeneous distribution of interparticle spacing within each segment (A). In contrast, for 5000 rpm (B) and 7000 rpm (C) spin coating speeds the edge of the nanotopography dominates the regular self-assembly of the nanoparticles within the segments. A strong enrichment of particles and thus a smaller spacing are observed at the edges of lower segments. SEM images of samples prepared with different spin coating speeds are provided in Figure S1 of the Supporting Information.

agreement with previously published studies.[11] The interparticle spacing appears to be almost homogeneous throughout each segment at a spin coating speed of 1000 rpm (Figure 4A). However, at higher RPM a significant accumulation of particles appears near the edges of lower segments of the quadruple (Figure 4B,C), and despite this accumulation, the difference in interparticle spacing between the centers of the segments is minor (Figure 4C). Likewise, the disorder in pattern hexagonality is restricted to a few hundred nanometers near the edges (Figure S3, Supporting Information). This illustrates the importance of selecting the optimum spin coating speed in this method. That is to say, low spin coating speeds yield larger interparticle spacing differences between the centers of different segments (here >20 nm between segments a and c for 1000 rpm, Figures 2B and 4A) as well as a more homogeneous particles distribution over the entire segment compared to higher speeds. Additionally, we were able to improve the nanoparticle distribution at the segment edges through ultrasound annealing, which followed the spin coating step (Figure S2, Supporting Information).

The nanopatterns generated with our method have the same chemical contrast as conventional nanoparticle arrays generated with BCML on flat substrates, hence standard protocols for the coupling of functional molecules can be used.[5,27] BCML can be applied to many different substrate types.[2,28,29] Also, the etching of regular nanotopographies has become a routine technique,[30] allowing straightforward transfer of our surface-coating strategy to substrates other than SiO_2 wafers.

4. CONCLUSIONS

We present a novel self-assembly fabrication method for quasi-hexagonal patterns of gold nanoparticles with well-defined interparticle spacing on microstructured substrates using diblock copolymer micelle nanolithography. The driving force for the observed topographic height-dependent interparticle spacing is attributed to immersion forces and steric interactions acting on the micelles during the evaporation of the solvent. Whereas it is known that nanoparticle structures on surfaces can be altered by surface topography,[31,32] the precise structure generated with such methods is difficult to control. On the contrary, our method combines the intriguing structural features of BCML with nanotopography-controlled arrangement, leading to hexagonally ordered micronanostructures by pure self-assembly. Hence, our strategy provides a high-throughput method to control the density and spacing of nanoparticles in micrometer-sized segments.

■ ASSOCIATED CONTENT

Supporting Information

The Supporting Information is available free of charge on the ACS Publications website at DOI: 10.1021/acs.langmuir.5b02168.

SEM images of nanoparticle patterns prepared at different spin coating speeds. Order parameter of quasi-hexagonal micronanostructures. SEM image showing the arrangement of nanoparticles on a micronanostructure. (PDF)

■ AUTHOR INFORMATION

Corresponding Author

*E-mail: cse@tf.uni-kiel.de.

Notes

The authors declare no competing financial interest.

■ ACKNOWLEDGMENTS

We acknowledge funding from the Deutsche Forschungsgemeinschaft (DFG) through the SFB 677 and grant SE 1801/2-1 as well as from the European Research Council (ERC starting grant no. 336104). C.L. is supported by a grant from the Marie Skłodowska Curie Actions Intra European Fellowship (PIEF-GA-2012-330418). We thank Joachim Spatz for his advice on block copolymer micelle nanolithography and Brook Shurtleff for proofreading the manuscript.

■ REFERENCES

(1) Spatz, J. P.; Mößmer, S.; Hartmann, C.; Möller, M.; Herzog, T.; Krieger, M.; Boyen, H.; Ziemann, P.; Kabius, B. Ordered Deposition of Inorganic Clusters from Micellar Block Copolymer Films. *Langmuir* **2000**, *16*, 407−415.

(2) Kruss, S.; Wolfram, T.; Martin, R.; Neubauer, S.; Kessler, H.; Spatz, J. P. Stimulation of Cell Adhesion at Nanostructured Teflon Interfaces. *Adv. Mater.* **2010**, *22* (48), 5499−5506.

(3) Graeter, S. V.; Huang, J.; Perschmann, N.; López-García, M.; Kessler, H.; Ding, J.; Spatz, J. P. Mimicking Cellular Environments by Nanostructured Soft Interfaces. *Nano Lett.* **2007**, *7* (5), 1413−1418.

(4) Lohmüller, T.; Helgert, M.; Sundermann, M.; Brunner, R.; Spatz, J. P. Biomimetic Interfaces for High-Performance Optics in the Deep-UV Light Range. *Nano Lett.* **2008**, *8* (5), 1429−1433.

(5) Selhuber, C.; Blümmel, J.; Czerwinski, F.; Spatz, J. P. Tuning Surface Energies with Nanopatterned Substrates. *Nano Lett.* **2006**, *6* (2), 267−270.

(6) Arnold, M.; Cavalcanti-Adam, E. A.; Glass, R.; Blümmel, J.; Eck, W.; Kantlehner, M.; Kessler, H.; Spatz, J. P. Activation of Integrin Function by Nanopatterned Adhesive Interfaces. *ChemPhysChem* **2004**, *5*, 383−388.

(7) Cavalcanti-Adam, E. A.; Volberg, R.; Micoulet, A.; Kessler, H.; Geiger, B.; Spatz, J. P. Cell Spreading and Focal Adhesion Dynamics Are Regulated by Spacing of Integrin Ligands. *Biophys. J.* **2007**, *92*, 2964−2974.

(8) Selhuber-Unkel, C.; López-García, M.; Kessler, H.; Spatz, J. P. Cooperativity in Adhesion Cluster Formation during Initial Cell Adhesion. *Biophys. J.* **2008**, *95*, 5424−5431.

(9) Möller, M.; Spatz, J. P.; Roescher, A. Gold nanoparticles in micellar poly(styrene)-b-poly(ethylene oxide) films−size and inter-particle distance control in monoparticulate films. *Adv. Mater.* **1996**, *8* (4), 337−340.

(10) Haupt, M.; Miller, S.; Ladenburger, A.; Sauer, R.; Thonke, K.; Spatz, J. P.; Riethmüller, S.; Möller, M.; Banhart, F. Semiconductor

DOI: 10.1021/acs.langmuir.5b02168
Langmuir 2015, 31, 9261−9265

nanostructures defined with self-organizing polymers. *J. Appl. Phys.* **2002**, *91* (9), 6057−6059.
(11) Arnold, M.; Hirschfeld-Warneken, V. C.; Lohmüller, T.; Heil, P.; Blümmel, J.; Cavalcanti-Adam, E. A.; López-García, M.; Walther, P.; Kessler, H.; Geiger, B.; Spatz, J. P. Induction of Cell Polarization and Migration by a Gradient of Nanoscale Variations in Adhesive Ligand Spacing. *Nano Lett.* **2008**, *8* (7), 2063−2069.
(12) Lohmueller, T.; Bock, E.; Spatz, J. P. Synthesis of Quasi-Hexagonal Ordered Arrays of Metallic Nanoparticles with Tuneable Particle Size. *Adv. Mater.* **2008**, *20* (12), 2297−2302.
(13) Chen, C. S.; Mrksich, M.; Huang, S.; Whitesides, G. M.; Ingber, D. E. Geometric Control of Cell Life and Death. *Science* **1997**, *276* (5317), 1425−1428.
(14) Blättler, T.; Huwiler, C.; Ochsner, M.; Städler, B.; Solak, H.; Vörös, J.; Grandin, H. M. Nanopatterns with Biological Functions. *J. Nanosci. Nanotechnol.* **2006**, *6* (8), 2237−2264.
(15) Krauss, T. N.; Barrena, E.; Lohmuller, T.; Spatz, J. P.; Dosch, H. Growth mechanisms of phthalocyanine nanowires induced by Au nanoparticle templates. *Phys. Chem. Chem. Phys.* **2011**, *13* (13), 5940−5944.
(16) Glass, R.; Arnold, M.; Blümmel, J.; Küller, A.; Möller, M.; Spatz, J. P. Micro-Nanostructured Interfaces Fabricated by the Use of Inorganic Block Copolymer Micellar Monolayers as Negative Resist for Electron-Beam Lithography. *Adv. Funct. Mater.* **2003**, *13* (7), 569−575.
(17) Aydin, D.; Schwieder, M.; Louban, I.; Knoppe, S.; Ulmer, J.; Haas, T. L.; Walczak, H.; Spatz, J. P. Micro-Nanostructured Protein Arrays: A Tool for Geometrically Controlled Ligand Presentation. *Small* **2009**, *5* (9), 1014−1018.
(18) Deeg, J. A.; Louban, I.; Aydin, D.; Selhuber-Unkel, C.; Kessler, H.; Spatz, J. P. Impact of Local versus Global Ligand Density on Cellular Adhesion. *Nano Lett.* **2011**, *11* (4), 1469−1476.
(19) Glass, R.; Arnold, M.; Cavalcanti-Adam, E. A.; Blümmel, J.; Haferkemper, C.; Dodd, C.; Spatz, J. P. Block copolymer micelle nanolithography on non-conductive substrates. *New J. Phys.* **2004**, *6* (1), 101.
(20) Glass, R.; Möller, M.; Spatz, J. P. Block copolymer micelle nanolithography. *Nanotechnology* **2003**, *14*, 1153−1160.
(21) Braun, D.; Fromherz, P. Fluorescence interference-contrast microscopy of cell adhesion on oxidized silicon. *Appl. Phys. A: Mater. Sci. Process.* **1997**, *65* (4−5), 341−348.
(22) Williges, C.; Chen, W.; Morhard, C.; Spatz, J. P.; Brunner, R. Increasing the Order Parameter of Quasi-Hexagonal Micellar Nanostructures by Ultrasound Annealing. *Langmuir* **2013**, *29* (4), 989−993.
(23) Rasband, W. S. *ImageJ*; U.S. National Institutes of Health: Bethesda, MD, 2005; http://rsb.info.nih.gov/ij/, Retrieved February 27, 2014.
(24) Zhang. Visualize Matrix by a Heatmap. *MATLAB Central File Exchange*; Retrieved June 12, 2015.
(25) Pavan, M. J.; Shenhar, R. Two-dimensional nanoparticle organization using block copolymer thin films as templates. *J. Mater. Chem.* **2011**, *21* (7), 2028−2040.
(26) Spatz, J. P. Nano- and Micropatterning by Organic−Inorganic Templating of Hierarchical Self-Assembled Structures. *Angew. Chem., Int. Ed.* **2002**, *41* (18), 3359−3362.
(27) Wolfram, T.; Belz, F.; Schoen, T.; Spatz, J. P. Site-specific presentation of single recombinant proteins in defined nanoarrays. *Biointerphases* **2007**, *2* (1), 44−48.
(28) Medda, R.; Helth, A.; Herre, P.; Pohl, D.; Rellinghaus, B.; Perschmann, N.; Neubauer, S.; Kessler, H.; Oswald, S.; Eckert, J.; Spatz, J. P.; Gebert, A.; Cavalcanti-Adam, E. A. Investigation of early cell−surface interactions of human mesenchymal stem cells on nanopatterned β-type titanium−niobium alloy surfaces. *Interface Focus* **2014**, *4* (1), 20130046.
(29) Schoen, T.; Wolfram, T.; Spatz, J. P. Magnesium-based Biodegradable Nanostructured Substrates: Hybrid Materials for Cellular Engraftment. *MRS Online Proc. Libr.* **2009**, *1235*, 1235-RR03-45.
(30) Köhler, M. *Wet-Chemical Etching Methods*. Wiley-VCH Verlag GmbH: 2007.
(31) Dai, Q.; Rettner, C. T.; Davis, B.; Cheng, J.; Nelson, A. Topographically directed self-assembly of goldnanoparticles. *J. Mater. Chem.* **2011**, *21* (42), 16863−16865.
(32) Mathur, A.; Brown, A.-D.; Erlebacher, J. Self-Ordering of Colloidal Particles in Shallow Nanoscale Surface Corrugations. *Langmuir* **2006**, *22* (2), 582−589.

DOI: 10.1021/acs.langmuir.5b02168
Langmuir 2015, 31, 9261−9265